Earth's Future

RESEARCH ARTICLE
10.1029/2020EF001626

Key Points:
- Hypersonic transport (HST) releasing nitrogen oxides and water vapor have the potential to reduce the stratospheric ozone abundance
- Per Tg injection of nitrogen oxides, the calculated ozone depletion is larger for aircraft flying at 30 km than 40 km altitude
- Ozone decrease near the HST flight altitude is reduced by about a third when temperature and dynamical feedbacks are taken into account

Supporting Information:
- Figure S1

Correspondence to:
G. Brasseur,
guy.brasseur@mpimet.mpg.de

Citation:
Kinnison, D., Brasseur, G. P., Baughcum, S. L., Zhang, J., & Wuebbles, D. (2020). The impact on the ozone layer of a potential fleet of civil hypersonic aircraft. *Earth's Future*, *8*, e2020EF001626. https://doi.org/10.1029/2020EF001626

Received 13 MAY 2020
Accepted 10 SEP 2020
Accepted article online 12 SEP 2020

Author Contributions:
Conceptualization: Douglas Kinnison, Guy P. Brasseur, Steven L. Baughcum
Formal analysis: Steven L. Baughcum, Jun Zhang
Methodology: Guy P. Brasseur
Software: Douglas Kinnison
Validation: Douglas Kinnison, Guy P. Brasseur
Writing - original draft: Douglas Kinnison, Guy P. Brasseur
Writing – review & editing: Steven L. Baughcum, Jun Zhang

The Impact on the Ozone Layer of a Potential Fleet of Civil Hypersonic Aircraft

Douglas Kinnison[1], Guy P. Brasseur[2], Steven L. Baughcum[1], Jun Zhang[3], and Donald Wuebbles[4]

[1]National Center for Atmospheric Research, Boulder, CO, USA, [2]Max Planck Institute for Meteorology, Hamburg, Germany, [3]Boeing Company, Seattle, WA, USA, [4]Department of Atmospheric Sciences, University of Illinois, Urbana, IL, USA

Abstract The aeronautical community is currently researching technology that might lead to commercial hypersonic aircraft that would cruise at Mach 5–8 in the middle or upper stratosphere and would transfer passengers from London to New York or from Los Angeles to Tokyo in just a couple of hours. Depending on the engine technology to be adopted, these aircraft will potentially release substantial amounts of water vapor and nitrogen oxides around 30–40 km altitude. We show here that the operation of a large fleet of such aircraft could potentially deplete considerable amounts of ozone in the stratosphere, which would lead to a substantial increase in biologically damaging ultraviolet radiation reaching the Earth's surface. The calculations are based on a specific emission scenario, which carries large uncertainties but can easily be scaled to account for the type of aircraft engine to be eventually adopted, improved technology to be expected, and the size and operation conditions of the future aircraft fleet.

Plain Language Summary Commercial hypersonic aircraft, if developed in the future, will be flying at Mach 5 to 8 in the middle to upper stratosphere (30 to 40 km altitude) to carry passengers in a couple of hours from London to New York or from Los Angeles to Tokyo. Depending on the adopted technology and fleet size, the powerful engines of such airplanes may release substantial amounts of water and nitrogen oxides in the stratosphere, which could potentially damage the protecting ozone layer and hence increase the level of biologically damaging ultraviolet radiation reaching the Earth surface. The paper uses an advanced global atmospheric model to assess the impact of a potential fleet of hypersonic aircraft.

1. Introduction

The aeronautical community is currently researching technology which might lead to the development of a fleet of commercial hypersonic transport (HST) at some time in the future. This new generation of aircraft with a 5,000 nautical mile range (about 9,000 km) would allow passengers to cross the Atlantic or the Pacific Ocean in just 2 to 3 hr at a speed of Mach 5–8. HST are expected to operate at or above 30 km altitude (100,000 feet), thus within or slightly above the protective ozone layer. The potential environmental impacts of such a fleet could be substantial and must therefore be assessed. Here, we focus on the ozone depletion that could result from the operation of an HST fleet.

In the 1970s, there was concern about the potential impact on stratospheric ozone (O_3) of a fleet of supersonic transport aircraft (SSTs flying typically at Mach 2–2.5) that was planned to operate in the decades ahead at an altitude of 15–20 km (Johnston, 1971). At the request of Congress in the United States, a crash program, the Climatic Impact Assessment Program (CIAP), was initiated by the Department of Transportation to provide a quantitative estimate of the climatic impact of these planned aircraft. Similar studies were conducted in other countries, including the United Kingdom, France, and Australia. The U.S. assessment (Grobecker et al., 1975) concluded that the emission of nitrogen oxides by a hypothetical fleet of 500 SSTs would not significantly affect the Earth's climate but would damage the ozone layer (Crutzen, 1972; Dameris et al., 1998; Hesstvedt, 1974; Johnston et al., 1989; McElroy et al., 1974; Tie et al., 1994).

The impact of current commercial subsonic aircraft, cruising in the upper troposphere (and in the lower stratosphere for flights occurring in polar regions), was assessed more recently (Brasseur et al., 1996, 1998, 2016; Lee et al., 2009; Penner et al., 1999; Schumann, 1994). Aviation CO_2 represents 2% to 3% of the total annual

CO_2 emissions. Nitrogen oxides released by jet engines generate additional ozone in the upper troposphere and therefore enhance radiative forcing. Condensation trails produced by the aircraft and the induced cirrus clouds also contribute to significant radiative perturbations (Penner et al., 1999). The overall radiative forcing by current commercial aviation is estimated to be of the order of 0.08 W/m^2 (Intergovernmental Panel for Climate Change, 2007).

The concept of commercial hypersonic aircraft is still under discussion, and no scenario about future aircraft emissions can be currently retained as representative of the future since these emissions depend on the type of engines to be adopted, the combustion system in such engines, the size of the future fleet, the conditions of operation including flight altitudes, and preferred routes of the aircraft. This study should therefore be viewed as an attempt to quantify the sensitivity of the stratospheric ozone concentration and of the ozone column abundance to localized emissions of nitrogen oxides and water vapor in the middle and upper stratosphere and hence to identify a possible threat to the biosphere (including humans) from the potential operation in the future of a fleet of hypersonic aircraft.

2. Emissions by Hypersonic Aircraft

Hypersonic aircraft are expected to operate at Mach 5–8 in an altitude range of 30–40 km (Yanes, 2020). The engine technology to be adopted remains a matter of debate, and intense research is conducted to investigate the advantages and disadvantages of different alternatives. One option under consideration is the adoption of air-breathing *ramjet* or *scramjet* engines. These engines use the fast motion of the aircraft to compress the incoming air rather than a built-in compressor as used in classic turbojet airliners. Acceleration from take-off to supersonic speeds must be achieved by another type of engine, for example, a turbojet engine burning hydrocarbon fuel or a rocket engine fueled by stored liquid oxygen and hydrogen. *Scramjets*, considered for aircraft operation at speeds higher than Mach 5, represent a modified version of the *ramjets* in which the air flows through the engine at supersonic speed, which improves the conversion of thermal energy into thrust. In one specific HST concept (Bowcutt, 2020), a turbofan jet engine, used to provide low-speed thrust during the initial part of the flight, is combined with an air-breathing *ramjet* to operate the vehicle at a hypersonic speed of Mach 5.

Other options are being considered. For example, the LAPCAT project (Steelant, 2008, 2011) was established by the European Commission to develop different hypersonic vehicle concepts, enabling an antipodal flight time to about 4 hr. One of the proposed configurations (LAPCAT-A2) was based on precooled turbo-*ramjet* fueled by hydrogen. The Synergetic Air Breathing Rocket Engine (SABRE), under consideration in the United Kingdom (Szondy, 2019), combines in a single system a conventional air-breathing jet engine (to be used for speed of less than approximately Mach 5) and a rocket engine (capable of accelerating the aircraft to speeds as high as Mach 25). The European STRATOFLY 300-passenger airliner was conceived to reach Mach 8 (European Commission, 2018) and would be equipped with two types of *ramjet* engines, one to be used for the first part of the flight up to the speed of Mach 4.5 and the second for flight operations from Mach 4.5 to Mach 8. A single cryogenically precooled air-breathing turbojet engine would operate from take-off to cruise speed of Mach 5 as part of the HST under consideration by the Japan Aerospace Exploration Agency (JAXA) (http://www.aero.jaxa.jp/eng/research/frontier/hst/). Air-breathing engines have a high fuel efficiency compared to rockets in terms of propulsion performance, but combustion produces carbon dioxide, nitrogen oxides, and water vapor that are released in the atmosphere.

The combustion products to be released in the atmosphere by the proposed engines are not well characterized and quantified because they depend on the technology to be adopted. Early estimates made in the 1970s for the *ramjet* engine (Letzberg, 1973; Petersen & Waters, 1972) during the CIAP Program suggested that, due to the high temperatures in the combustion chamber, the emission index (EI) for nitrogen oxides (NO*x*) should be an order of magnitude greater than that of classic turbojets. The CIAP study adopted for the air-breathing engines of Concorde and of a hypothetical American SST an EI of 18 grams of NO_2 emitted per kg of fuel burned. Letzberg (1973) estimated that the EI for a *ramjet* would vary from 40 to 300 g NO_2 per kg of fuel for Mach numbers ranging from 5 to 12. That report also indicated that the amount of nitrogen oxides produced in the HST flow field by the shock wave occurring around the nose of the aircraft would be an order of magnitude lower than the emission by a *ramjet* engine, thus of the same order as the

Table 1
Hypersonic Transport Scenarios

Scenario	Altitude of injection	Species injected	Comments
Reference	NA	None	No subsonic emissions
HST-30 km-H_2O	30 km	H_2O only	EI(H_2O) = 1,237 g/kg fuel
HST-30 km-NO*x*	30 km	NO_2 only	EI(NO_2) = 20 g/kg fuel
HST-30 km-Comb	30 km	H_2O and NO_2	
HST-40 km-H_2O	40 km	H_2O only	EI(H_2O) = 1,237 g/kg fuel
HST-40 km-NO*x*	40 km	NO_2 only	EI (NO_2) = 20 g/kg fuel
HST-40 km-Comb	40 km	H_2O and NO_2	

emission by a classic turbojet. Brooks et al. (1993) indicate that, for Mach numbers between 1 to 10, the effect of NO output produced by the high-temperature boundary layer of the HST can be neglected compared to the emission by the engines. At Mach 16, however, the output of NO from the boundary layer of the aircraft would become roughly equal to the emission from a *scramjet* engine, and thus considerably higher than the emission of a classic air-breathing turbojet.

Letzberg (1973) also provides the emission for hydrogenated species per kg of fuel burnt: 500 to 900 g of H_2O, 19 to 300 g of H_2, and 38 to 333 g of OH, depending on the speed of the aircraft. Chemical kinetics computations (Grobecker et al., 1975) show that, due to the small value of the EI (OH)/EI (NO*x*) ratio, the conversion of nitrogen oxides to nitric acid is small. It can be therefore assumed that nitrogen compounds resulting from the combustion are emitted as nitric oxide. Finally, one should emphasize that the emission indices quoted in these early studies are very uncertain and can only be used as guides for future studies; they may represent overestimates if new engines benefit from advanced technology and optimized modes of operation.

Because of the large uncertainties existing on the number of aircraft to be deployed, the engine technology to be adopted, and the emission indices to be achieved in modern combustion chambers, we present here sensitivity studies that illustrate the potential impact of a hypothetical fleet of future hypersonic aircraft on the chemical composition of the atmosphere and specifically on the ozone abundance. The results produced for specific emissions can be easily scaled and adapted to represent the conditions that could prevail in the future. The model simulations presented in this paper should therefore be considered as providing a guide for the developers of hypersonic aircraft engines. In the present study, we only consider the key drivers of ozone change, specifically the emissions by aircraft engines of nitrogen oxides and water vapor. The contribution of molecular hydrogen is implicitly included in the water vapor emissions since both compounds, when oxidized, initiate the formation of the hydroxyl radical that catalytically destroys the ozone molecule.

For our model simulations and due to the lack of reliable data, we assume that the geographical distribution of the HST routes and the HST emissions are identical to the scenario adopted for a fleet of 500 stratospheric SSTs (Baughcum et al., 1998; Baughcum & Henderson, 1998; Kawa et al., 1999), operating at Mach 2.4 at 17–20 km altitude, but we assume that the injection of NO*x* and water vapor by the proposed HST takes place around 30 km (Case 1) or around 40 km altitude (Case 2) in a thin layer of about 2 km. We assume (Table 1) that 129 million kg of fuel is burned each day by the HST fleet with emission indices for water vapor and nitrogen oxides of 1,237 g H_2O/kg fuel burned and of 20 g NO_2/kg fuel burned, respectively. The corresponding total HST emissions for water vapor and nitrogen oxides are therefore equal to 58.3 Tg (H_2O)/year and 0.94 Tg (NO_2)/year, respectively. Note that in the adopted scenarios, about 84% of the HST emissions are taking place in the Northern Hemisphere. The total Northern Hemisphere emissions are therefore 48.8 Tg (H_2O)/year and 0.79 Tg (NO_2)/year. For comparison with natural processes as simulated by our model, which is described in section 3, the total natural atmospheric production of water vapor by methane oxidation and of nitrogen oxides by nitrous oxide oxidation is 60 Tg (H_2O)/year and 2.8 Tg (NO_2)/year, respectively. All these values represent orders of magnitude; in the case of water specifically, it is assumed here that the oxidation of background methane leads to two molecules of water. This number is, however, only approximate since it does not account for the part of methane diverted to the production of molecular hydrogen primarily in the mesosphere (Le Texier & Solomon, 1988) and for other chemical processes that reduce the water production yield to about 1.7 in the lower stratosphere (Frank et al., 2018).

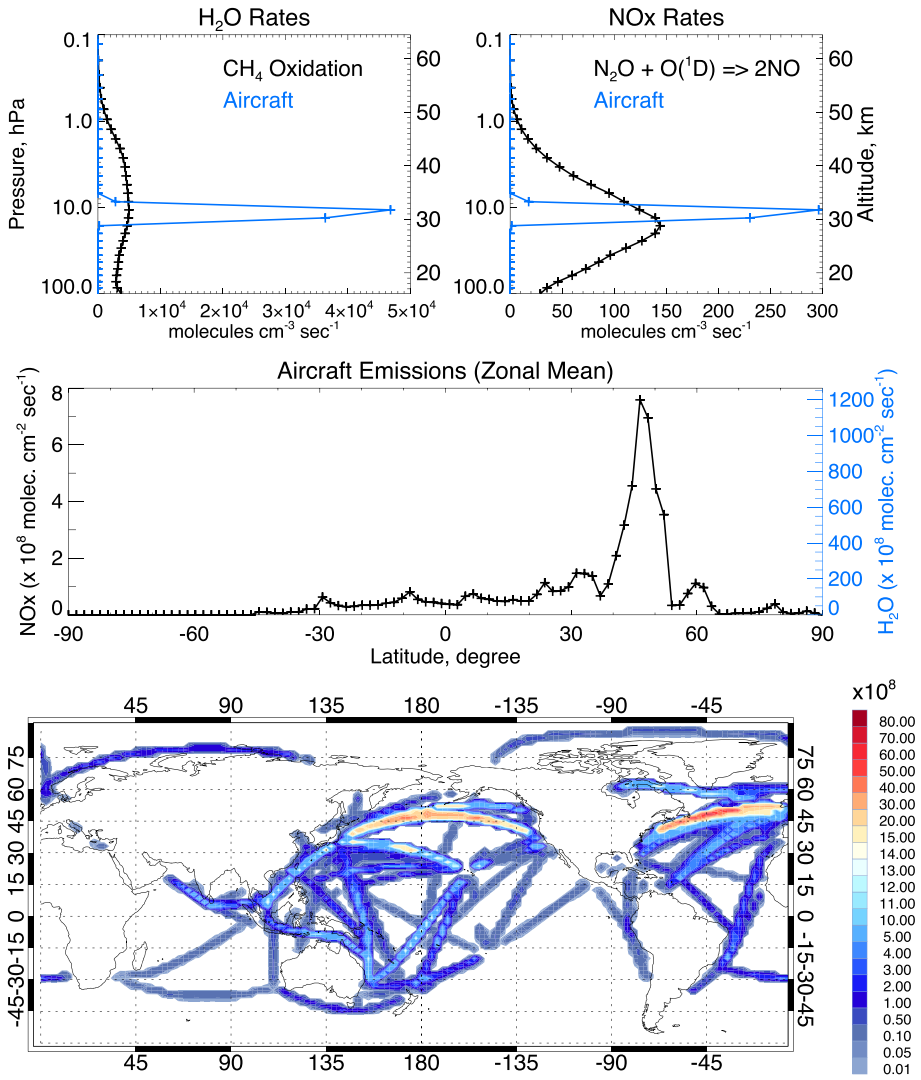

Figure 1. Upper panels: Adopted injection rates of global average water vapor and nitrogen oxides (molecules cm^{-3} s^{-1}) by a fleet of hypersonic aircraft assumed to operate at 30 km altitude. These perturbations are compared with the natural stratospheric photochemical production of water vapor (left) resulting from the oxidation of methane and of nitrogen oxides (right) resulting from the oxidation of nitrous oxide. The values are represented as global averages. Middle panel: Zonal mean vertically integrated aircraft emissions of NO*x* (left panel) and H_2O (right panel) as a function of latitude (molecules cm^{-2} s^{-1}). Lower panel: Geographical distribution of the emission of nitrogen oxides (molecules cm^{-2} s^{-1}) by a fleet of hypersonic transport as adopted for the model simulations in the present study.

In our simulations, the release of water and nitrogen oxides is assumed to take place primarily above the oceans, where most of the hypersonic flights will take place. Figure 1 shows that, with the adopted emissions, the stratospheric injection of water vapor and nitrogen oxides by the fleet of aircraft is larger than the natural atmospheric production of these species at the planned flight levels. The figure also highlights two prominent corridors in which high HST traffic is expected to occur: the northern Atlantic and Pacific Oceans.

3. Model Description

We derive the impact of these emissions on the global atmosphere by using the Community Earth System Model version 1 (CESM1), Whole Atmosphere Community Climate Model (WACCM) for the 2050 period. WACCM is a coupled chemistry-climate model ranging from the Earth's surface to the lower thermosphere (Garcia et al., 2007; Marsh et al., 2013). WACCM is a vertical extension of the Community Atmosphere

Model version 4 (CAM4) and includes all of the physical parameterizations of CAM4 (Neale et al., 2013) and a finite-volume dynamical core (Lin, 2004) for the tracer advection. The horizontal resolution is 1.9° latitude × 2.5° longitude. The vertical resolution in the lower stratosphere ranges from 1.2 km near the tropopause to about 2 km near the stratopause; in the mesosphere and thermosphere, the vertical resolution is ~3 km. Simulations used in the work are based on the International Global Atmospheric Chemistry/Stratosphere-troposphere Processes And their Role in Climate (IGAC/SPARC) Chemistry Climate Model Initiative (CCMI) (Morgenstern et al., 2017). Improvements in CESM1 (WACCM) for CCMI include a modification to the orographic gravity wave forcing that reduced the cold bias in Antarctic polar temperatures (Calvo et al., 2017; Garcia et al., 2007) and updates to the stratospheric heterogeneous chemistry which improved the representation of polar ozone depletion (Solomon et al., 2015; Wegner et al., 2013). The chemistry used in this version of WACCM is representative of the troposphere through the lower mesosphere (Kinnison et al., 2007; Tilmes et al., 2016). The species included within this mechanism are contained within the O*x*, NO*x*, HO*x*, ClO*x*, and BrO*x* chemical families, along with CH_4 and its degradation products. In addition, 20 primary nonmethane hydrocarbons and related oxygenated organic compounds are represented along with their surface emissions. There is a total of 183 species and 472 chemical reactions; this includes 17 heterogeneous reactions on multiple aerosol types (i.e., sulfate, nitric acid trihydrate, and water-ice). In this work, the baseline scenario follows the CCMI REF-C2 definition (Morgenstern et al., 2017), where the model is coupled to an interactive ocean. This scenario includes forcing of greenhouse gases (CH_4, N_2O, and CO_2), organic halogens, volcanic surface area density and heating, and 11-year solar cycle variability. The Quasi-Biennial Oscillation (QBO) is nudged to observed monthly mean tropical winds from the 86 to 4 hPa levels (Matthes et al., 2010). For the simulations shown here, the model is branched off of an existing REF-C2 simulation in year 2040 and run through year 2050. High-frequency meteorological fields are output instantaneously every 3 hr. In addition, sea surface temperatures and sea ice from this branched run are derived. With this information, the reference period and HST simulations are run in a specified dynamics (SD) mode (Kunz et al., 2011; Lamarque et al., 2012). Here, temperature, zonal and meridional winds, and surface pressure are used to drive the physical parameterization that control boundary layer exchanges, advective and convective transport, and the hydrological cycle. These meteorological fields are nudged from the surface to 125 km, with a 5-hr relaxation time constant. The goal here is to have all scenarios have identical temperature and transport distributions from the surface through the mesosphere. Table 1 shows the scenarios used in this work. All simulations considered in the present study were carried out for a period of 11 years; the results presented below represent the annual average of the last year of model integration.

4. The Response of Ozone to the HST Injection of Water Vapor and Nitrogen Oxides

It is well known that the destruction of odd oxygen (O*x* = O_3 + O + $O(^1D)$ + other terms; Brasseur & Solomon, 2005) is catalyzed by nitrogen oxides in the stratosphere (Crutzen, 1970, 1979) and by hydroxyl radicals in the upper stratosphere and mesosphere (Bates & Nicolet, 1950). The simultaneous release of both types of compounds could lead to chemical interactions that could mitigate the effects of the individual emissions on ozone destruction. For example, the injection of water vapor contributes to the conversion into nitric acid of a fraction of aircraft generated reactive NO*x*. Reactive ozone-depleting chlorine (e.g., ClO) produced by the photochemical degradation of industrially manufactured chlorofluorocarbons is partly destroyed by the addition of nitrogen oxides released by the HST aircraft engines. However, this effect will gradually become less pronounced as the atmospheric levels of anthropogenic chlorine are expected to decrease in the coming decades. In this study, we have adopted a level of total stratospheric chlorine of 2.3 ppbv, the concentration expected to be representative for the 2050 time period. This is a decrease of ~35% from the peak near year 2000.

We illustrate the response of the atmospheric composition to the injection by a potential HST fleet by displaying the change in the zonal and annual mean concentration (expressed in percent) of water vapor, nitrogen oxides, and ozone. Figure 2 shows the percentage increase in the water vapor concentration of the stratosphere resulting from the operation of the HST fleet. This scenario assumes that the cruise altitude of the aircraft is 30 km. The largest perturbation (larger than 30% or ~3.5 ppmv) in H_2O takes place between 30° and 70°N, although the noticeable effect of the water emissions reaches the North Pole, the equator, and

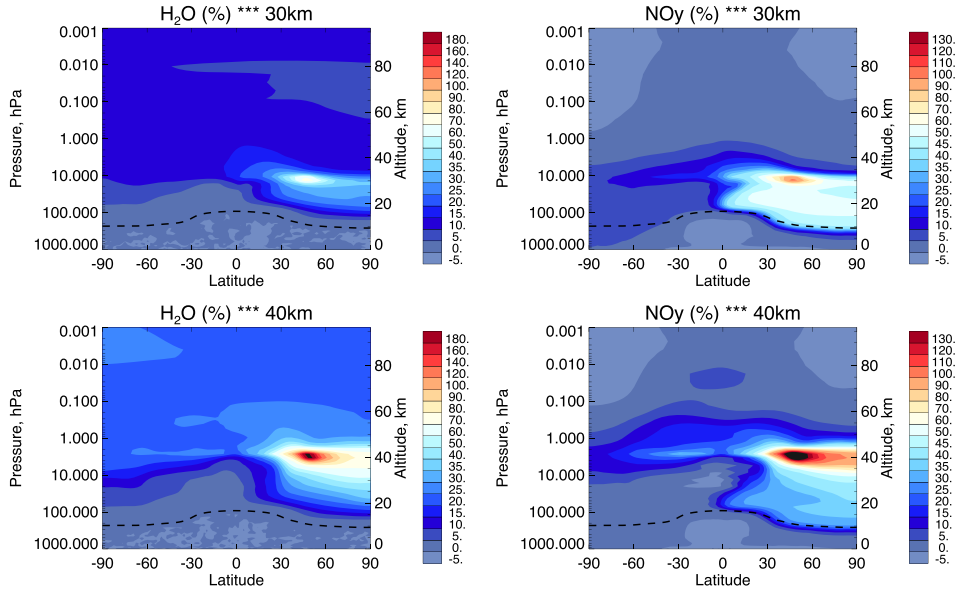

Figure 2. Annual and zonal mean perturbations (percent) in the atmospheric concentrations of H_2O (left panels) and NO*y* (right panels) for an injection by a fleet of HST cruising at 30 km (upper panels) and 40 km altitude (lower panels). The dashed black line is the location of the lapse rate tropopause.

even the Southern Hemisphere. At midlatitudes in the Northern Hemisphere, the altitude range of the perturbation extends from 15 km (25 km in the tropics) to about 40 km.

When the altitude of the injection (with the same emission) is located at 40 km altitude, the maximum perturbation for H_2O reaches 140% (10 ppmv). The atmospheric region affected by the emission of water extends from 20 to 60 km in the northern midlatitudes and from 35 to 60 km in the tropics. It also affects most of the Southern Hemisphere with some small effect (20%) between 30 and 70 km. Interestingly, the predicted increase of water vapor reaches 5–15% in the upper mesosphere/lower thermosphere.

The perturbations in total odd nitrogen (noted NO*y* and defined as the sum of N + NO + NO_2 + NO_3 + HO_2NO_2 + HNO_3 + $2N_2O_5$ + $ClONO_2$ + minor contributions from other nitrogen species) are also shown in Figure 2 for aircraft emissions occurring at the cruise altitudes of 30 and 40 km, respectively. In the first case, the relative perturbation is largest (50–90%) between 15 and 35 km at middle and high latitudes and from 20 to 40 km in the tropics (40–60%). In the second case, the altitude with the largest relative perturbations ranges from 30 to 45 km (up to 300% increase) and from 35 to 60 km at midlatitudes and in the tropics, respectively. In each case, a tongue of elevated NO*y* extends in the Southern Hemisphere to about 70°S.

It is interesting to note that only a relatively small fraction of the material emitted by the aircraft's engines in the Northern Hemisphere is transported and dispersed south of the equator. Interhemispheric exchanges occur with a time constant of about 1 to 1.5 years (Bowman & Cohen, 1997; Geller et al., 1997) due to the strong upwelling that takes place in the equatorial region (Plumb & Eluszkiewicz, 1999; Randel et al., 2002). Tracers injected into the lower or middle stratosphere are therefore transported to higher levels before being transported across the equator.

Figure 3 depicts the background water vapor distribution and the increase in the water vapor mixing ratio in response to the aircraft injection at 30 km. The figure also shows that the loss rate of H_2O (expressed in ppmv/year) is very small below 30 km but increases above this level where the photolysis of this molecule becomes possible by the penetration in the upper atmosphere of shortwave ultraviolet solar radiation. The lifetime of water vapor is larger than 1 year below 40 km altitude and larger than 10 years below 30 km. The transformation of water molecules released in the atmosphere by hypersonic aircraft into ozone-depleting reactive hydrogen radicals (H, OH, and HO_2) is therefore slow in the stratosphere but becomes efficient in the mesosphere and lower thermosphere for the water molecules that are transported up to these altitudes. At 80 km, the lifetime of H_2O is only of the order of 10 days, and large amounts of hydrogen radicals are formed.

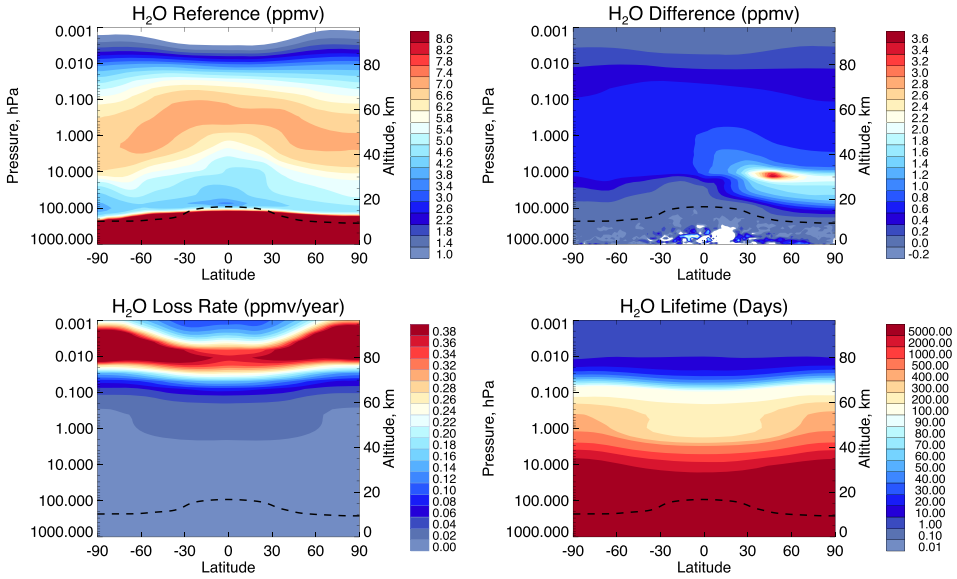

Figure 3. Upper panels: Background atmospheric mixing ratio of water vapor (left) and increase in H_2O due to aircraft emission (right) (both in ppmv). Lower panels: Loss rate of H_2O resulting primarily from the photolysis of water by solar ultraviolet radiation. (left; ppmv/year) and H_2O lifetime (days). All panels represent annual and zonal averages.

As shown by Figure 4, the perturbation in HO*y* (defined as the sum $H + OH + HO_2 + 2H_2O_2 + 2\,H_2 + 2H_2O$) generated by the aircraft emissions is most pronounced near the location of the emissions at 30 km in the Northern Hemisphere; a limited intrusion toward the Southern Hemisphere occurs, however, in the upper stratosphere and lower mesosphere. Figure S1 in the supporting information shows the 40 km injection altitude result. When we contrast the behavior of HO*x* defined as the sum of all hydrogen species without water

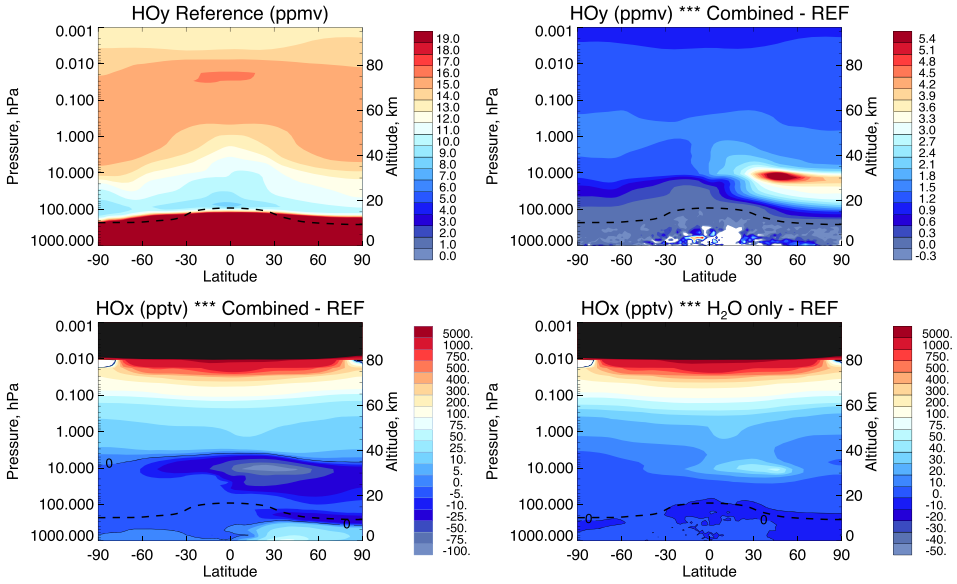

Figure 4. First-row (top) panels: Reference annual and zonal mean distribution of HO*y* mixing ratio (ppmv) defined as the sum of the $H + OH + HO_2 + 2H_2O_2 + 2\,H_2 + 2H_2O$ mixing ratios (left); perturbation in the annual and zonal mean HO*y* mixing ratio (ppmv) resulting from the combined injection of water vapor and nitrogen oxides by HST at 30 km altitude (right). Second-row panels: Perturbation in the annual and zonal mean HO*x* mixing ratio (ppmv), where $HOx = H + OH + HO_2 + 2H_2O_2$, resulting from the combined injection of water vapor and nitrogen oxides by HST at 30 km altitude (left); same as for the left panel, but for H_2O-only injection (right).

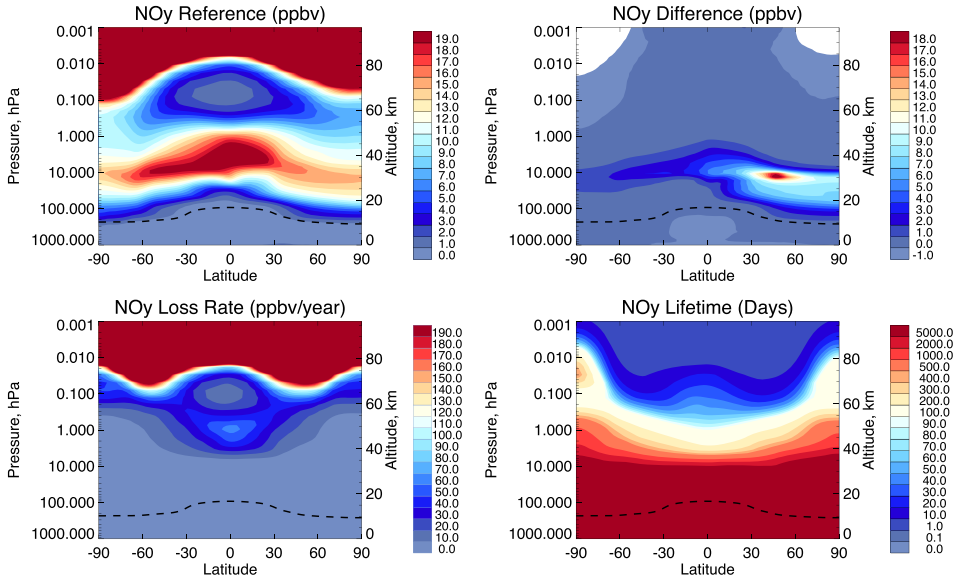

Figure 5. Upper panels: Background atmospheric mixing ratio of NO*y* (=N + NO + NO_2 + 2 N_2O_5 + HNO_3 + other minor contributions) (left) and increase in NO*y* due to aircraft emission at 30 km (right) (both in ppbv). Lower panels: Loss rate of NO*y* resulting from the photolysis of nitric oxide by solar ultraviolet radiation followed by the recombination of N and NO (left; ppbv/year) and NO*y* lifetime (days) relative to the N + NO destruction process. All panels represent annual and zonal averages.

vapor and molecular hydrogen included (HO*x* = HO*y* − 2 H_2 − 2 H_2O) with the behavior of the total HO*y*, we note that the increase in HO*x* is largest (of the order of 1 ppm) above 80 km altitude, but it is very small in the stratosphere. In fact, as shown by the two lower panels in Figure 4, the change in the HO*x* concentration in the lower stratosphere is positive in the case of an H_2O-only injection. It is negative, however, in the case of a combined (H_2O, NO*x*) emission since the nitrogen oxides released by the aircraft tend to convert HO*x* into nitric acid. In summary, water vapor injected by aircraft should not destroy substantial amounts of ozone in the stratosphere, but the material injected transported upward should destroy a significant quantity of ozone and atomic oxygen in the lower thermosphere with very small effects on the ozone column abundance.

In the case of NO*y* (Figure 5), the situation is somewhat similar to that of water vapor but with some quantitative differences. Odd nitrogen is destroyed by the photolysis of NO in the upper stratosphere, mesosphere, and lower thermosphere (producing N and O), followed by the recombination of N with NO to form molecular nitrogen (N_2). The lifetime of NO*y* of more than 10 years in the lower stratosphere is reduced to less than 3 months above 40 km, a value that is smaller than the interhemispheric transport time scale. In this case, the transport of NO*y* across the tropical region to the Southern Hemisphere is therefore somewhat hampered by the existence of NO*y* loss process.

The six panels in Figure 6 show the change in zonal and annual mean ozone concentration resulting from the emissions at 30 and 40 km of water vapor, nitrogen oxides, and both combined. When only water vapor emissions are considered, the largest percent ozone reduction is found around 80 km, where ozone is very sensitive to the hydroxyl and hydroperoxyl radicals. The maximum depletion is 9% when the emissions are occurring at 30 km and 20% when they are located at 40 km. For an injection of water at 30 km, the ozone reduction is typically 2% at the stratopause (50 km) and 5% around 60–70 km altitude. A slight ozone increase of 1% calculated near 30 km latitude results from the self-healing effect of the ozone layer (Solomon et al., 1985). In the case of pure NO*x* emissions, the ozone reduction is larger than 10% between 20 and 35 km altitude (between 30 and 40 km in the tropics) for a 30 km injection and between 20 and 45 km (between 35 and 45 km in the tropics) for an injection at 40 km. The peak ozone reduction is 30% and 37%, respectively.

When considering the combined effects of NO*x* and H_2O emissions, we calculate a maximum reduction in the zonal annual mean ozone concentration of the order of 25% (1.5 ppmv) and of 35% (2.5 ppmv) for flight altitudes of 30 and 40 km, respectively.

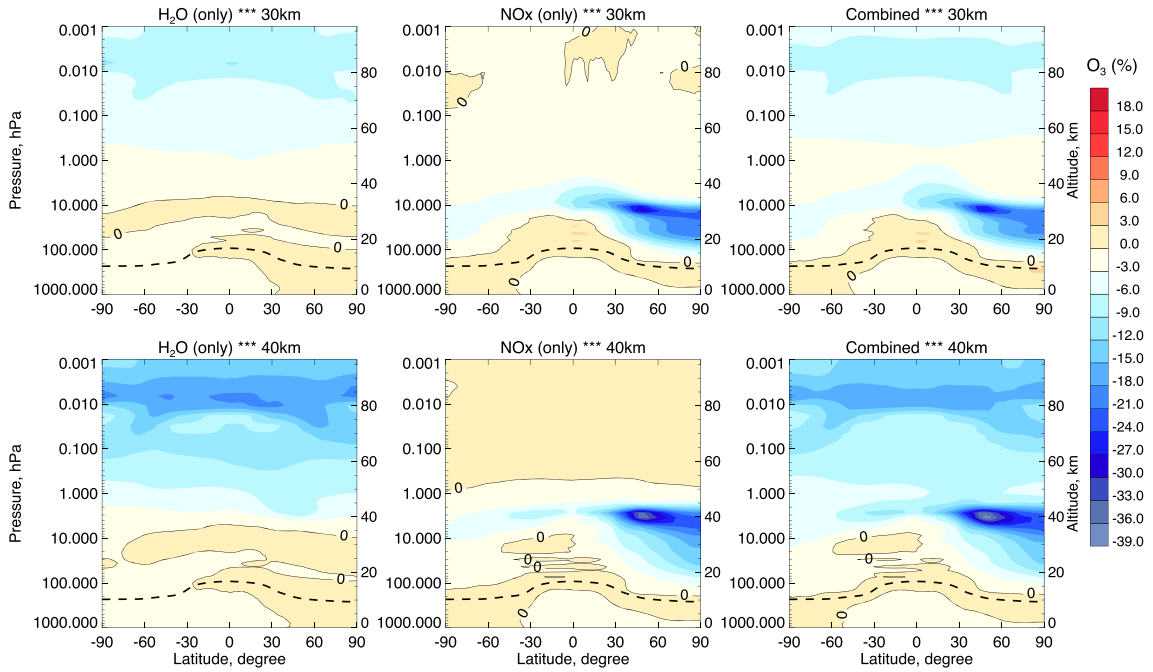

Figure 6. Percent change in the atmospheric concentration of ozone for an injection of H_2O (left panels), NO*x* (middle panels), and combined NO*x* + H_2O (right panels) by a fleet of HST operating at 30 km (upper panels) and 40 km (lower panels), respectively.

The change in the ozone column for individual and combined injections of water vapor and nitrogen oxides at 30 and 40 km is shown in Figure 7 as a function of latitude and season. As expected, the largest depletion of ozone takes place in the Northern Hemisphere, where most aircraft operate. At the high northern latitudes, the reduction in the ozone column is of the order of 8–10% (25 Dobson units) for a 30 km injection

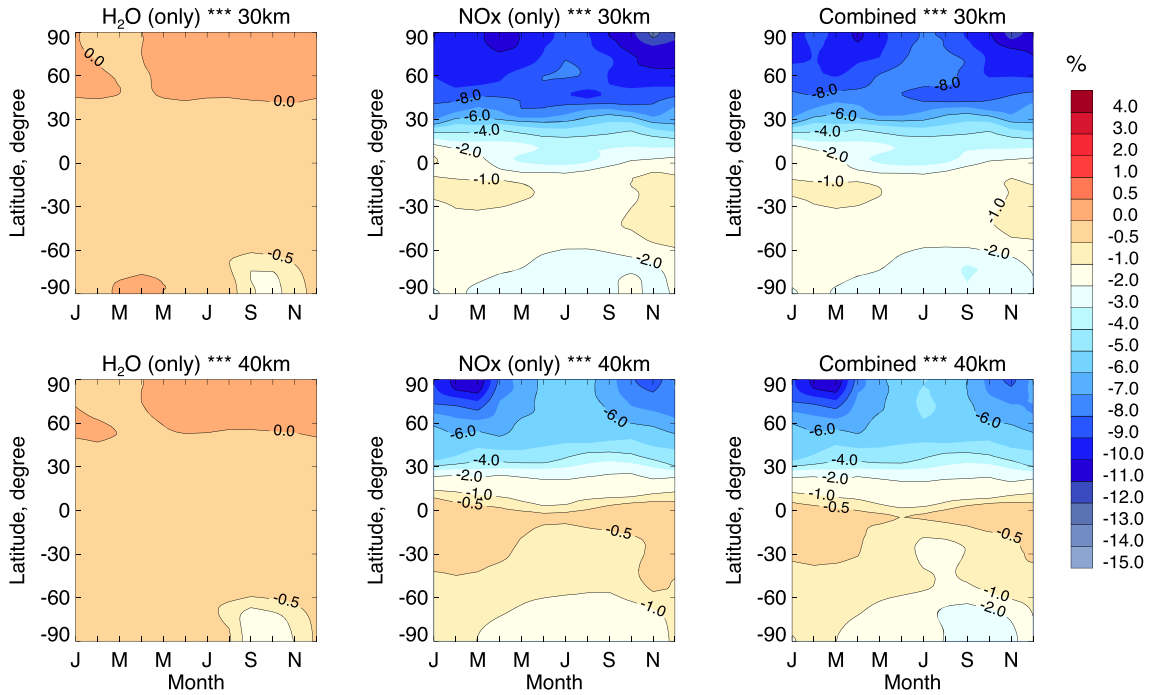

Figure 7. Calculated reduction in the ozone column as a function of latitude and month of the year calculated for an injection of water vapor (left panels) and nitrogen oxides (middle panels) and for the combined emissions (right panels) by the adopted HST fleet cruising at 30 km (upper panels) and 40 km (lower panels), respectively.

Table 2
Global (GL) and Northern Hemispheric (NH) Change in the Ozone Column (in Dobson Units or DU and in Percent) and Sensitivity of the Ozone Column to a Global and Hemispheric HST Injection of 0.789 Tg (NO_2)/year and 0.942 Tg (NO_2)/year in the NH and GL, Respectively

Domain	Reference ozone column	Altitude of injection	Calculated ozone column	Difference due to HST	Difference due to HST	Ozone sensitivity	Ozone sensitivity
	DU	km	DU	DU	%	DU/Tg NO_2	%/Tg NO_2
Global	290.4	30	278.9	−11.5	−4.0	−11.8	−4.2
Global	290.4	40	283.8	−6.5	−2.2	−6.9	−2.4
NH	305.1	30	285.7	−19.4	−6.3	−24.5	−8.0
NH	305.1	40	293.7	−11.4	−3.7	−14.5	−4.7

and close to 5–8% (20 Dobson units) for a 40 km injection. Most of the ozone reduction is due to the release in the atmosphere of NO*x*. The maximum percentage reduction (10–12%) occurs in the polar region in spring and fall. The maximum reduction at high latitudes in the Southern Hemisphere is of the order of 2%. Again, these quantitative values are directly linked to the adopted emission scenarios.

In order to provide values with little dependence on the adopted magnitude of emissions by HST, we present in Tables 2 and 3 the global and Northern Hemispheric average ozone reduction relative to an annual injection per Tg of NO*x* and per Tg of H_2O, respectively. Note that these ozone changes refer to emissions integrated over the entire Earth and the Northern Hemisphere, respectively. All presented values are annual average, zonal mean, for year 2050.

These tables show that, per Tg/year of injected substance, the ozone column is considerably more sensitive to nitrogen oxide than water vapor. The ozone reduction in response to water vapor takes place primarily in the upper atmosphere with little effect on the ozone column. Further, the ozone sensitivity to nitrogen oxides is larger when the flight altitude is located at 30 rather than 40 km. We note, in particular, that per Tg/year of injected NO_2 at 30 km injection, the average ozone depletion calculated in the Northern Hemisphere is as large as 24.5 DU or 8%. For an injection at 40 km, this reduction is 14.5 DU or 4.7%. Reductions can be locally larger, specifically at high latitudes.

Finally, in order to assess the perturbation in the chemical budget of odd oxygen as a function of altitude, we show in Figure 8 the Northern Hemisphere annual averaged change in the different contributions to the O*x* loss rate function of altitude. The top panels depict the loss rates for a 2050 reference atmosphere, in percent of total O*x* loss and in absolute value. They show that at the cruise altitude planned for the HST, more than 50% of the background ozone loss results from the catalytic destruction by NO*x*. The contribution by water vapor becomes dominant only above 45 km altitude and remains such in the upper atmosphere.

Figure 8 also shows that the injection by aircraft of water or nitrogen oxides modifies the O*x* loss rate by other reactive species, which highlights the existence of chemical interactions between the different ozone catalytic destruction cycles. This is especially evident for the 40 km injections (i.e., H_2O only, NO*x* only, and combined). Here the H_2O only simulation increases HO*x* (see Figure S1) and increases the HO*x* family chemical loss (bottom row, left panel of Figure 8). The increase in HO*x* decreases the NO*x* family chemical loss by the reaction of OH + NO_2 forming nitric acid (HNO_3). This process is converting the more

Table 3
Global (GL) and Northern Hemispheric (NH) Change in the Ozone Column (in Dobson Units or DU and in Percent) and Sensitivity of the Ozone Column to a Global and Hemispheric HST Injection of 48.83 Tg (H_2O)/year and 58.25 Tg (H_2O)/year in the NH and GL, Respectively

Domain	Reference ozone column	Altitude of injection	Calculated ozone column	Difference due to HST	Difference due to HST	Ozone sensitivity	Ozone sensitivity
	DU	km	DU	DU	%	DU /Tg H_2O	% /Tg H_2O
Global	290.4	30	290.1	−0.30	−0.10	−0.005	−0.002
Global	290.4	40	290.0	−0.39	−0.13	−0.007	−0.002
NH	305.1	30	305.0	−0.16	−0.05	−0.003	−0.001
NH	305.1	40	304.9	−0.23	−0.08	−0.005	−0.002

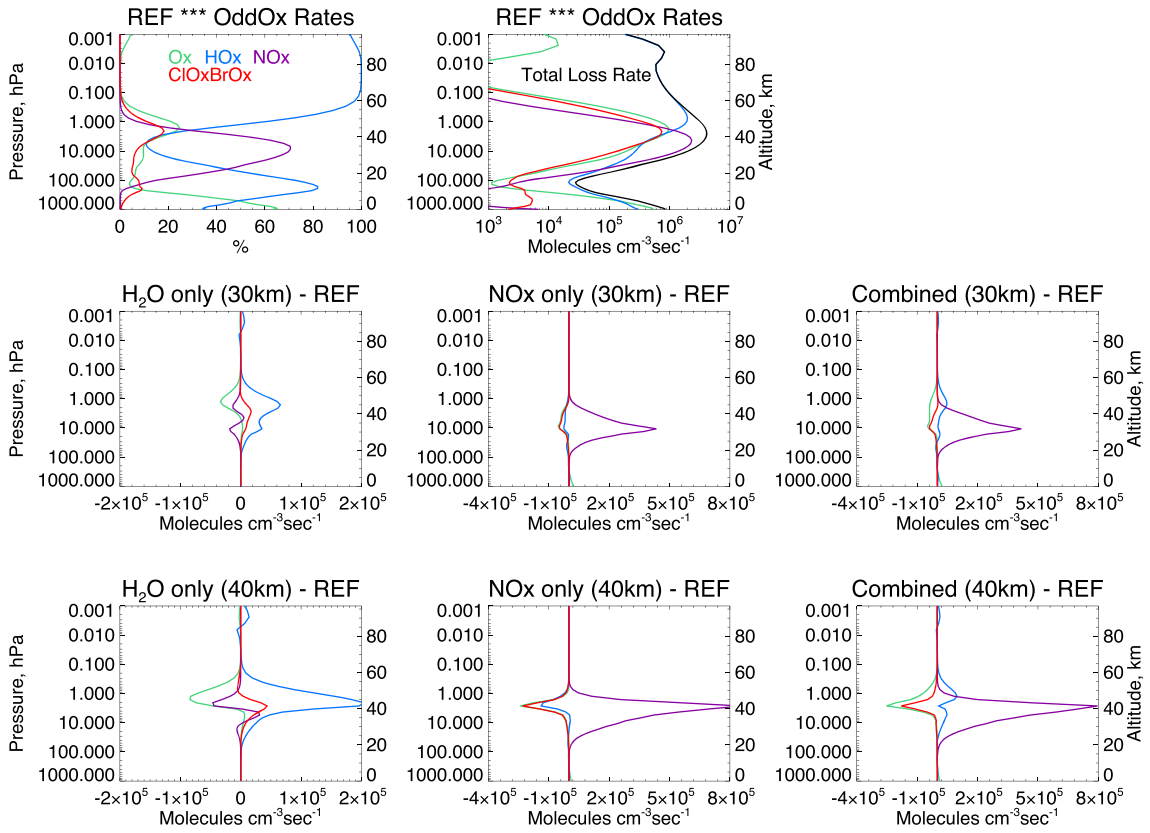

Figure 8. Top panel: Chemical loss rates (Northern Hemisphere average profiles) of odd oxygen by the Chapman destruction mechanism (O*x*) and by catalytic cycles involving nitrogen oxides (NO*x*), hydrogen radicals (HO*x*), halogen oxides (ClO*x*/BrO*x*). The different contributions are expressed in percent of the total loss rate (left) and in molecules cm^{-3} s^{-1} (right). Middle panel: Change in the odd oxygen destruction rate (molecules cm^{-3} s^{-1}) in response to the adopted injection of water (left) and nitrogen oxides (right) by HST at 30 km altitude. Bottom panel: Same as the middle panel but for an injection at 40 km altitude. For the definition of odd oxygen used in this study ($Ox = O3 + O(^3P) + O(^1D) + NO_2 + 2NO_3 + HNO_3 + HO_2NO_2 + 2N_2O_5 + ClO + 2Cl_2O_2 + 2OClO + 2ClONO_2 + BrO + 2\ BrONO_2$, which is approximatively equal to $O_3 + O(^3P)$) and the reactions that are contained in each odd oxygen chemical family, see page 414, Chapter 5 of Brasseur and Solomon (2005).

catalytically active NO_2 molecule into a longer-lived molecule (HNO_3) and therefore reducing the overall NO*x* family odd oxygen loss. When NO*x* only is emitted, the O*x*, ClO*x*, BrO*x*, and HO*x* odd oxygen loss families all decrease relative to the H_2O only simulation. Again, this is due to interfamily coupling reactions removing active odd oxygen loss species from these families. However, the overall all odd oxygen loss increases due to the NO*x* family, and substantial ozone depletion is derived (Figures 6 and 7).

5. Chemical-Dynamical Interactions

The results described in the previous sections are based on model simulations in which the dynamical fields (winds and temperature) are specified as model input and are therefore insensitive to changes in the chemical composition of the atmosphere and specifically to the HST injection. Deriving the full dynamical response to changes in stratospheric ozone concentrations and specifically the response of the atmospheric circulation to the HST operations requires comprehensive Earth system model simulations in which the dynamics of the atmosphere is simulated consistently with changes in chemical and related radiative processes ("online model"). Due to the internal dynamical variability of the atmosphere, an ensemble of several (typically 10 or more) model realizations with slightly different initial conditions should be produced for the background atmosphere as well as for the two perturbed cases. Such computationally expensive ensemble could be performed as part of a more extensive modeling assessment exercise. Here, in order to highlight the potential importance of temperature and circulation feedbacks, we perform two additional simulations in which chemical-dynamical interactions are taken into account in a reference case and in a perturbed case (with a 30 km

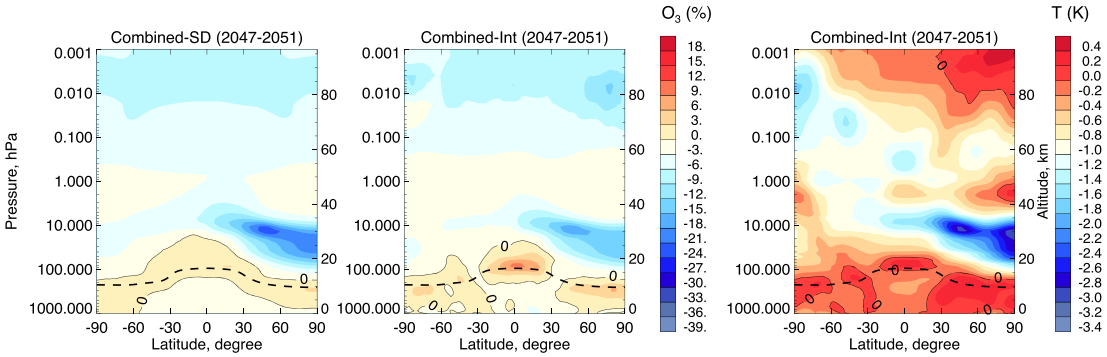

Figure 9. Zonally and multiannually (2047 to 2051) averaged response of ozone and temperature to the constant injection at 30 km of water vapor and nitrogen oxides by the fleet of hypersonic aircraft as defined in the text. Left panel: ozone change (percent) derived from a model simulation with specified dynamics (SD). Middle panel: same but for a free-running model case (FR) with interactive dynamics. Right panel: Change in temperature (Kelvin) obtained from the free-running model. A weak filter has been applied along the vertical to damp small noisy features appearing in the FR case.

injection by the HST fleet as considered in the previous sections), respectively. Although only one realization of the model dynamics is represented for each case, these two free-running (FR) calculations provide some information on the magnitude of interannual variability, the perturbation in the temperature structure with the related slow-down of the catalytic ozone destruction, the change in the strength of the Brewer-Dobson circulation, and with the intrusion of water vapor through the cold trap of the tropical tropopause.

The differences between the time variation of ozone derived by specified dynamics and calculated dynamics are substantial. For example, in the Arctic at 78°N, the relative difference in the ozone column abundance between the perturbed and background cases during the last 5 years of the model integration varies from −7% to −11% in the SD case and from +8% and −23% in the FR case (the difference between two single realizations). When averaged over a period of 5 years (model years 2047 to 2051) to reduce the effect of interannual variability, the changes in the zonally averaged ozone concentration and temperature are those represented in Figure 9. First, as expected, in the FR case, we note a cooling of the Northern Hemisphere upper stratosphere that reaches 3 K at 30 km altitude. This temperature decrease results from a reduction in the absorption of solar ultraviolet radiation by ozone. The mean ozone depletion calculated in the FR simulation is smaller than in the SD case (maximum ozone reduction of 18% versus 28%) due to a large extent to the positive relationship between photochemical ozone destruction and temperature.

Large differences between the specified dynamics and free-running cases are also noticeable in the vicinity of the tropopause where large vertical ozone gradients and a long chemical lifetime makes ozone particularly sensitive to dynamical variability. Stone et al. (2018) showed from an ensemble of model simulations that the response of ozone to external perturbations is very variable in the lower stratosphere, particularly in the tropics. In the realization shown in Figure 9, the ozone concentration increases by up 5% in the vicinity of the tropopause. This value could be very different in other model realizations.

6. Conclusions

As shown by the model simulations presented here, a fleet of hypersonic aircraft that is being considered for future intercontinental travel has the potential to substantially reduce the atmospheric column abundance if sufficiently large amounts of nitrogen oxides are released in the atmosphere. The impact of water vapor on the ozone column is found to be considerably smaller. The study shows that, for a given amount of emissions, the impact on ozone is larger if the flight altitude is located at 30 km (closer to the ozone maximum) rather than 40 km altitude. As expected, the effects are more pronounced in the Northern Hemisphere, where the largest fraction of the fleet will be operated. However, due to the long-range transport aircraft effluents and probable local emissions, the potential effects on ozone in the Southern Hemisphere cannot be ignored. The calculated ozone depletion is largest in the polar region of the Northern Hemisphere and is most pronounced in spring (March and April) and fall (October and November). In the Southern Hemisphere, its largest effect occurs in Antarctica during the period of the ozone hole formation, but the amplitude is considerably lower than the ozone reduction associated with the development of hole.

The projections derived with a free-running chemistry-climate model show qualitatively the same results as the simulations performed with fixed dynamics. However, the maximum ozone depletion resulting from the injection of engine effluents at 30 km altitude is reduced by about a third due to the chemistry/temperature feedback in this region of the stratosphere. Further, the ozone response in the vicinity of the tropopause appears to be strongly affected by dynamical variability. A full analysis of the mean ozone change near the tropopause should be performed on the basis of an ensemble of a large number of model realizations.

The impact on the atmosphere of a potential future fleet of hypersonic aircraft will depend on the fleet size, the type of operations, the fuel consumption by each aircraft, the type of fuel to be used, and the emission indices for the different effluents released by the engines. If HST engines release nitrogen oxides in substantial quantity, the average level of biologically harmful ultraviolet radiation (UV-B) radiation could increase and produce detrimental effects on the biosphere; in particular, it could enhance the number of skin cancers affecting humans.

Data Availability Statement

Model results shown in this paper are available online (at https://acomstaff.acom.ucar.edu/dkin/EarthsFuture_Kinnison_2020).

Acknowledgments
WACCM is a component of the Community Earth System Model (CESM), which is supported by the National Science Foundation. We would like to acknowledge high-performance computing support from Cheyenne (doi:10.5065/D6RX99HX) provided by NCAR's Computational and Information Systems Laboratory, sponsored by the National Science Foundation. The University of Illinois representation in this study is supported in part by the Boeing Company.

References

Bates, D. R., & Nicolet, M. (1950). The photochemistry of atmospheric water vapor. *Journal of Geophysical Research*, *55*, 301–326. https://doi.org/10.1029/jz055i003p00301

Baughcum, S. L., & Henderson, S. C. (1998). *Aircraft emission scenarios projected in year 2015 for the NASA Technology Concept Aircraft (TCA) High Speed Civil Transport (NASA Contract Report CR-1998-207635)*. Hampton, VA: National Aeronautics and Space Administration.

Baughcum, S. L., Henderson, S. C., & Sutkus, D. J. (1998). *Scheduled civil aircraft emission inventories projected for 2015: Database development and analysis (NASA Contract CR-1998-207,638)*. Hampton, VA: National Aeronautics and Space Administration.

Bowcutt, K. G. (2020). Flying at the edge of space and beyond: The opportunities and challenges of hypersonic flight. *The Bridge*, *50*, 51–58. Retrieved from https://www.nae.edu/theBridge

Bowman, K. P., & Cohen, P. J. (1997). Interhemispheric exchange by seasonal modulation of the Hadley circulation. *Journal of the Atmospheric Sciences*, *54*, 2045–2059. https://doi.org/10.1175/1520-0469(1997)054<2045:IEBSMO>2.0.CO;2

Brasseur, G. P., Cox, R. A., Hauglustaine, D., Isaksen, I., Lelieveld, J., Lister, D. H., et al. (1998). European scientific assessment of the atmospheric effects of aircraft emissions. *Atmospheric Environment*, *32*, 2327–2422. https://doi.org/10.1016/s1352-2310(97)00486-x

Brasseur, G. P., Gupta, M., Anderson, B., Balasubramanian, S., Barrett, S., Duda, D., et al. (2016). Impact of aviation on climate, FAA's Aviation Climate Change Research Initiative (ACCRI) Phase II. *Bulletin of the American Meteorological Society*, *97*, 561–583. https://doi.org/10.1175/bams-d-13-00089.1

Brasseur, G. P., Müller, J.-F., & Granier, C. (1996). Atmospheric impact of NO_x emissions by subsonic aircraft: A three-dimensional study. *Journal of Geophysical Research*, *101*, 1423–1428. https://doi.org/10.1029/95jd02363

Brasseur, G. P., & Solomon, S. (2005). *Aeronomy of the middle atmosphere, Atmospheric and Oceanographic Science Library* (Vol. 32). Dordrecht, The Netherlands: Springer.

Brooks, S. B., Lewis, J. M., & Dickerson, R. R. (1993). Nitric oxide emissions from high-temperature viscous boundary layers of hypersonic aircraft within the stratosphere. *Journal of Geophysical Research*, *98*, 16,755–16,760. https://doi.org/10.1029/93JD01237

Calvo, N., Garcia, R. R., & Kinnison, D. E. (2017). Revisiting Southern Hemisphere polar stratospheric temperature trends in WACCM: The role of dynamical forcing. *Geophysical Research Letters*, *44*, 3402–3410. https://doi.org/10.1002/2017GL072792

Crutzen, P. (1970). The influence of nitrogen oxides on the atmospheric ozone content. *Quarterly Journal of the Royal Meteorological Society*, *96*, 320–325. https://doi.org/10.1002/qj.49709640815

Crutzen, P. (1979). The role of NO and NO_2 in the chemistry of the troposphere and stratosphere. *Annual Review of Earth and Planetary Sciences*, *7*, 443–472. https://doi.org/10.1146/annurev.ea.07.050179.002303

Crutzen, P. J. (1972). *SST's: A threat to the Earth's ozone shield, Ambio* (Vol. 1, pp. 41–51). Heidelberg, Germany: Springer.

Dameris, M., Grewe, V., Köhler, I., Sausen, R., Brühl, C., Grooß, J.-U., & Steil, B. (1998). Impact of aircraft NO_x emissions on tropospheric and stratospheric ozone. Part II: 3-D model results. *Atmospheric Environment*, *32*, 3185–3199. https://doi.org/10.1016/s1352-2310(97)00505-0

European Commission (2018). *Stratospheric flying opportunities for high-speed propulsion concepts, EC-H2020*. Brussels, Belgium: European Union.

Frank, F., Jöckel, P., Gromov, S., & Dameris, M. (2018). Investigating the yield of H_2O and H_2 from methane oxidation in the stratosphere. *Atmospheric Chemistry and Physics*, *18*, 9955–9973. https://doi.org/10.5194/acp-18-9955-2018

Garcia, R. R., Marsh, D., Kinnison, D. E., Boville, B., & Sassi, F. (2007). Simulations of secular trends in the middle atmosphere, 1950–2003. *Journal of Geophysical Research*, *112*, D09301. https://doi.org/10.1029/2006JD007485

Geller, L. S., Elkins, J. W., Lobert, J. M., Clarke, A. D., Hurst, D. F., Butler, J. H., & Myers, R. C. (1997). Tropospheric SF6: Observed latitudinal distribution and trends, derived emissions and interhemispheric exchange time. *Geophysical Research Letters*, *24*(6), 675–678. https://doi.org/10.1029/97GL00523

Grobecker, A. J., Coroniti, S. C., & Cannon, R. H. Jr. (1975). *Report of findings, Report DOT-TSC-75-50*. Washington, DC: US Dept. of Transportation.

Hesstvedt, E. (1974). Reduction of stratospheric ozone from high-flying aircraft, studied in a two-dimensional photochemical model with transport. *Canadian Journal of Chemistry*, *52*(8), 1592–1598. https://doi.org/10.1139/v74-231

Intergovernmental Panel for Climate Change (2007). *Climate change: The physical science basis. Contribution of Working Group I to the Fourth Assessment Report*. Cambridge, UK: Cambridge University Press.

Johnston, H. (1971). Reduction of stratospheric ozone by nitrogen oxide catalysts from supersonic transport exhaust. *Science*, *173*, 517–522. https://doi.org/10.1126/science.173.3996.517

Johnston, H. S., Kinnison, D. E., & Wuebbles, D. J. (1989). Nitrogen oxides from high-altitude aircraft: An update of potential effects on ozone. *Journal of Geophysical Research*, *94*, 16,351–16,363. https://doi.org/10.1029/jd094id13p16351

Kawa, S. R., Anderson, J. G., Baughcum, S. L., Brock, C. A., Brune, W. H., Cohen, R. C., et al. (1999). *Assessment of the effects of high-speed aircraft in the stratosphere: 1998* (NASA Technocal Paper TP-1999-209, Vol. 237). Washington, DC: National Aeronautics and Space Administration.

Kinnison, D. E., Brasseur, G. P., Walters, S., Garcia, R. R., Sassi, F., Boville, B. A., et al. (2007). Sensitivity of chemical tracers to meteorological parameters in the MOZART-3 chemical transport model. *Journal of Geophysical Research*, *112*, D20302. https://doi.org/10.1029/2006JD007879

Kunz, A., Pan, L., Konopka, P., Kinnison, D., & Tilmes, S. (2011). Chemical and dynamical discontinuity at the extratropical tropopause based on START08 and WACCM analysis. *Journal of Geophysical Research*, *116*, D24302. https://doi.org/10.1029/2011JD016686

Lamarque, J. F., Emmons, L. K., Hess, P. G., Kinnison, D. E., Tilmes, S., Vitt, F., et al. (2012). CAM-chem: Description and evaluation of interactive atmospheric chemistry in the Community Earth System Model. *Geoscientific Model Development*, *5*, 369–411. https://doi.org/10.5194/gmd-5-369-2012

Le Texier, H., Solomon, S., & Garcia, R. R. (1988). The role of molecular hydrogen and methane oxidation in the water vapor budget. *Quarternaly Journal of the Royal Meteorological Society*, *114*, 281–295. https://doi.org/10.1002/qj.49711448002

Lee, D. S., Fahey, D. W., Forster, P. M., Newton, P. J., Wit, R. C. N., Lim, L. L., et al. (2009). Aviation and global climate change in the 21st century. *Atmospheric Environment*, *43*, 3520–3537. https://doi.org/10.1016/j.atmosenv.2009.04.024

Letzberg, E. A. (1973). *Emission calculations for a scramjet powered hypersonic transport* (NASA Technical Memorandum X-71464). Cleveland, OH: National Aeronautics and Space Administration.

Lin, S.–J. (2004). A "vertically-Lagrangian" finite-volume dynamical core for global atmospheric models. *Monthly Weather Review*, *132*, 2293–2307. https://doi.org/10.1175/1520-0493(2004)132<2293:AVLFDC>2.0.CO;2

Marsh, D. R., Mills, M. J., Kinnison, D. E., Lamarque, J.-F., Calvo, N., & Polvani, L. M. (2013). Climate change from 1850 to 2005 simulated in CESM1(WACCM), 73,727,391. *Journal of Climate*, *26*(19). https://doi.org/10.1175/JCLI-D-12-00558.1

Matthes, K., Marsh, D. R., Garcia, R. R., Kinnison, D. E., Sassi, F., & Walters, S. (2010). Role of the QBO in modulating the influence of the 11-year solar cycle on the atmosphere using constant forcings. *Journal of Geophysical Research*, *115*, D18110. https://doi.org/10.1029/2009JD013020

McElroy, M. B., Wofsy, S. C., Penner, J. E., & McConnell, J. C. (1974). Atmospheric ozone, possible impact of stratospheric aviation. *Journal of the Atmospheric Sciences*, *31*, 287–303. https://doi.org/10.1175/1520-0469(1974)031<0287:AOPIOS>2.0.CO;2

Morgenstern, O., Hegglin, M. I., Rozanov, E., O'Connor, F. M., Abraham, N. L., Akiyoshi, H., et al. (2017). Review of the global models used within phase 1 of the Chemistry-Climate Model Initiative (CCMI). *Geoscientific Model Development*, *10*, 639–671. https://doi.org/10.5194/gmd-10-639-2017

Neale, R. B., Richter, J., Park, S., Lauritzen, P. H., Vavrus, S. J., Rasch, P. J., & Zhang, M. (2013). The mean climate of the Community Atmosphere Model (CAM4) in forced SST and fully coupled experiments. *Journal of Climate*, *26*(5), 5150–5168. https://doi.org/10.1175/jcli-d-12-00236.1

Penner, J. E., Lister, D. H., Griggs, D. J., Dokken, D. J., & McFarland, M. (Eds). (1999). *Aviation and the global atmosphere* (pp. 1–373). Cambridge, UK: Cambridge University Press.

Petersen, R. H., & Waters, M. H. (1972). Hypersonic transports economics and environmental effects. NASA TM. *Journal of Aircraft*, *10*, X-62193. https://doi.org/10.2514/3.44372

Plumb, R. A., & Eluszkiewicz, J. (1999). The Brewer-Dobson circulation: Dynamics of the tropical upwelling. *Journal of the Atmospheric Sciences*, *56*, 868–890. https://doi.org/10.1175/1520-0469(1999)056<0868:tbdcdo>2.0.co;2

Randel, W. J., Garcia, R. R., & Wu, F. (2002). Time-dependent upwelling in the tropical lower stratosphere estimated from the zonal-mean momentum budget. *Journal of the Atmospheric Sciences*, *59*, 2141–2152. https://doi.org/10.1175/1520-0469(2002)059<2141:tduitt>2.0.co;2

Schumann, U. (1994). On the effect of emissions from aircraft engines on the state of the atmosphere. *Annales de Geophysique*, *12*, 365–384. https://doi.org/10.1007/s00585-994-0365-0

Solomon, S., Garcia, R. R., & Stordal, F. (1985). Transport processes and ozone perturbations. *Journal of Geophysical Research*, *90*, 12,981–12,989. https://doi.org/10.1029/jd090id07p12981

Solomon, S., Kinnison, D. E., Bandoro, J., & Garcia, R. (2015). Simulations of polar ozone depletion: An update. *Journal of Geophysical Research*, *120*, 7958–7974. https://doi.org/10.1002/2015JD023365

Steelant, J. (2008). *LAPCAT: High-speed propulsion technology* (Educational Notes NATO RTO-EN-AVT-150). Reston, VA: North Atlantic Treaty Organization.

Steelant, J. (2011). *Sustained hypersonic flight in Europe: First technology achievements within LAPCAT II*. Paper presented at 17th AIAA International Space Planes and Hypersonic Systems and Technologies Conference, American Institute for Aeronautics and Astronautics, Reston, VA. https://doi.org/10.2514/6.2011-2243

Stone, K. A., Solomon, S., & Kinnison, D. E. (2018). On the identification of ozone recovery. *Geophysical Research Letters*, *45*, 5158–5165. https://doi.org/10.1029/2018GL077955

Szondy, D. (2019). *Airbreathing SABER Rocket engine set to enter test phase*. Retrieved from https://newatlas.com/air-breathing-sabre-engine-testing/58874/

Tie, X. X., Brasseur, G., Lin, X., Friedlingstein, P., Granier, C., & Rasch, P. (1994). The impact of high-altitude aircraft on the ozone layer in the stratosphere. *Journal of Atmospheric Chemistry*, *18*, 103–128. https://doi.org/10.1007/BF00696810

Tilmes, S., Lamarque, J.-F., Emmons, L. K., Kinnison, D., Marsh, D., Garcia, R. R., et al. (2016). Representation of the Community Earth System Model (CESM1) CAM4-Chem within the Chemistry-Climate Model initiative. *Geoscientific Model Development*, *9*, 1853–1890. https://doi.org/10.5194/gmd-9-1853-2016

Wegner, T., Kinnison, D. E., Garcia, R. R., & Solomon, S. (2013). Simulation of polar stratospheric clouds in the specified dynamics version of the Whole Atmosphere Community Climate Model. *Journal of Geophysical Research*, *118*, 4991–5002. https://doi.org/10.1002/jgrd.50415

Yanes, J. (2020). *The future of aviation*. Madrid, Spain: OpenMind BBVA. Retrieved from https://www.bbvaopenmind.com/en/technology/future/hypersonic-the-future-of-aviation